GEOPHYSICS, VOL. 88, NO. 4 (JULY-AUGUST 2023); P. A19–A23, 5 FIGS.
10.1190/GEO2023-0024.1

Optimized time-lapse acquisition design via spectral gap ratio minimization

Yijun Zhang[1], Ziyi Yin[1], Oscar López[2], Ali Siahkoohi[3], Mathias Louboutin[1], Rajiv Kumar[4], and Felix J. Herrmann[1]

ABSTRACT

Modern-day reservoir management and monitoring of geologic carbon storage increasingly call for costly time-lapse seismic data collection. We demonstrate how techniques from graph theory can be used to optimize acquisition geometries for low-cost sparse 4D seismic data. Based on midpoint-offset-domain connectivity arguments, our algorithm automatically produces sparse nonreplicated time-lapse acquisition geometries that favor wavefield recovery.

INTRODUCTION

Time-lapse seismic data acquisition is a costly but crucial endeavor for reservoir management and monitoring of geologic carbon storage. Although a sparse randomized collection of seismic data can lead to major improvements in acquisition productivity (Hennenfent and Herrmann, 2008; Herrmann and Hennenfent, 2008; Herrmann, 2010; Mosher et al., 2014), systematic approaches to performance prediction, other than computationally expensive simulation-based studies, are mostly lacking. In addition, acquisition optimization approaches, such as minimizing the mutual coherence (Tang et al., 2008; Mosher et al., 2014; Obermeier and Martinez-Lorenzo, 2017) or minimizing the spectral gap ratio (SGR) (Zhang et al., 2022; López et al., 2023), do not handle the unique challenges of time-lapse seismic data acquisition.

To meet these challenges, inversion with the joint recovery model (JRM) (Oghenekohwo et al., 2017; Wason et al., 2017) will be combined with automatic binary sampling mask generation driven by SGR minimization (Zhang et al., 2022). We opt for the JRM because it inverts the baseline and monitor surveys jointly for the common component, which contains information shared between the surveys, and innovations with respect to the common component. Because the fictitious common component is observed by all surveys, its recovery improves when the time-lapse surveys contain complementary information. This is the case in which sparse surveys are not replicated (Oghenekohwo et al., 2017; Wason et al., 2017) or the time-lapse data sets contain independent noise terms (Tian et al., 2018). In either case, the JRM leads without insisting on replication of the surveys to high degrees of time-lapse repeatability in the data (Oghenekohwo et al., 2017; Wason et al., 2017) and image space (Yin et al., 2023). It also yields better interpretability of time-lapse field data (Wei et al., 2018).

As demonstrated in this paper, including the common component offers additional advantages when optimizing time-lapse acquisition via SGR minimization. To demonstrate this, we first explain the relationship between the SGR and connectivity within graphs associated with binary sampling masks. Next, we describe how this connectivity, which favors wavefield reconstruction, can be improved by minimizing the SGR via optimization. To enhance the inversion of time-lapse data with the JRM, a new optimization objective will be introduced that contains SGRs of the common component and the baseline/monitor surveys. After a brief discussion on minimizing this objective with simulated annealing, the proposed methodology for automatic time-lapse binary mask generation is numerically validated on realistic synthetic 2D data.

OPTIMIZED TIME-LAPSE ACQUISITION

Although the SGR has been used successfully to predict and improve the performance of wavefield reconstruction, it has not yet been used to optimize time-lapse acquisition. After briefly discussing the SGR and JRM, we introduce our methodology to optimize time-lapse data acquisition.

Manuscript received by the Editor 11 January 2023; revised manuscript received 17 March 2023; published ahead of production 20 April 2023; published online 20 June 2023.
[1]Georgia Institute of Technology, Atlanta, Georgia, USA. E-mail: yzhang3198@gatech.edu (corresponding author); ziyi.yin@gatech.edu; mlouboutin3@gatech.edu; felix.herrmann@gatech.edu.
[2]Harbor Branch Oceanographic Institute, Fort Pierce, Florida, USA. E-mail: oscarfabianlopez@gmail.com.
[3]Rice University, Houston, Texas, USA. E-mail: alisk@rice.edu.
[4]Schlumberger, London, UK. E-mail: rkumar19@slb.com.

DOI:10.1190/geo2023-0024.1

The spectral gap ratio

As shown by López et al. (2023), the success of seismic data wavefield reconstruction via universal matrix completion (Bhojanapalli and Jain, 2014) can be predicted by the ratio of the first two singular values of binary sampling masks $\sigma_2(\mathbf{M})/\sigma_1(\mathbf{M}) \in [0,1]$, where $\mathbf{M}$ is a binary matrix with ones where data are sampled and with zeros otherwise. This ratio is known as the SGR and provides a cheap-to-compute quantitative measure to predict recovery quality. The smaller the SGR, the better the connectivity within graphs spanned by binary sampling masks. Improved connectivity leads to improved wavefield recovery (López et al., 2023). Although useful, the SGR itself is not constructive because it does not produce sampling masks with small SGRs. With simulated annealing, Zhang et al. (2022) devise a practical algorithm to generate acquisition geometries with small SGRs. In this work, we extend this approach by optimizing sparse geometries for time-lapse data acquisition.

Optimized sampling mask generation

Given an initial binary mask, $\mathbf{M} \in \{0,1\}^{n_s \times n_r}$, with n_s sources and n_r receivers, Zhang et al. (2022) propose a methodology to minimize the SGR via

$$\underset{\mathbf{M}}{\text{minimize}}\ \mathcal{L}(\mathbf{M}) \quad \text{subject to } \mathbf{M} \in \mathcal{C}, \tag{1}$$

with the objective, $\mathcal{L}(\mathbf{M}) = \sigma_2(\mathbf{M})/\sigma_1(\mathbf{M})$, given by the SGR. To ensure the feasibility of the optimized binary masks with source subsampling ratio $\rho \in (0,1)$, the constraint $\mathcal{C} = \bigcap_{i=1}^{3} \mathcal{C}_i$ is included, which consists of the intersection of the cardinality constraint, $\mathcal{C}_1 = \{\mathbf{M} | (\mathbf{M}) = \lfloor n_s \times \rho \rfloor \times n_r\}$, the binary mask constraint, $\mathcal{C}_2 = \{\mathbf{M} | \mathbf{M} \in \{0,1\}^{n_s \times n_r}\}$, and a constraint on the maximum gap size between consecutive samples, $\mathcal{C}_3 = \{\mathbf{M} | \text{maxgap}(\mathbf{M}) \leq \Delta\}$, where Δ is the maximal permitted gap size. By solving equation 1, Zhang et al. (2022) produce binary sampling masks that improved wavefield reconstruction compared with masks generated by randomized jittered sampling (Hennenfent and Herrmann, 2008). Figure 1 contrasts jittered with optimized sampling in the midpoint-offset domain, reducing the SGR from 0.333 to 0.196. The optimized mask increases the sampling at the near offsets where there are more ways to connect to midpoints, which favors wavefield reconstruction (López et al., 2023). This paper delves deeper into time-lapse survey design and proposes a novel simulation-free method to find near-optimal sparse source locations for a baseline survey and one or more monitor survey(s). Our method is guided by the JRM, which has a successful track record in time-lapse wavefield reconstruction (Oghenekohwo et al., 2017; Wason et al., 2017). Next, we introduce the JRM and present our SGR minimization framework, which is tailored to optimize the time-lapse survey design in accordance with the JRM.

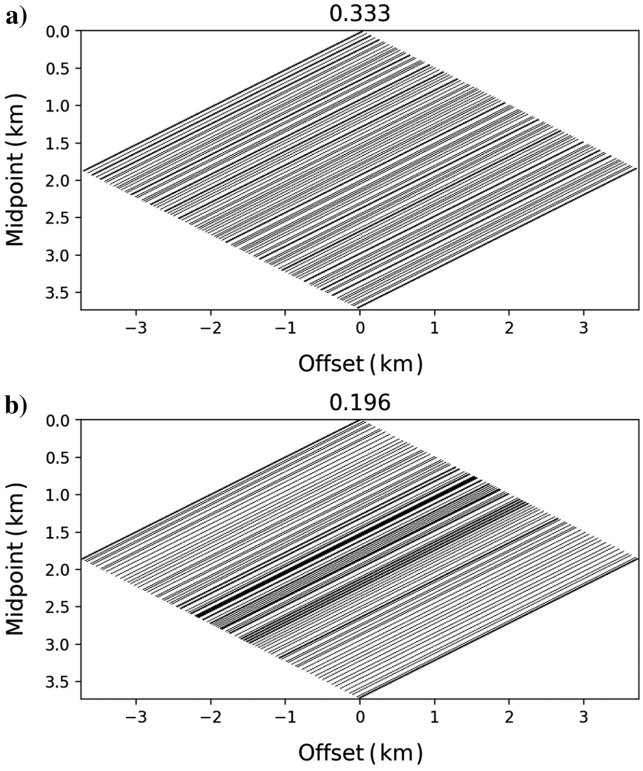

Figure 1. (a) Jittered versus (b) optimized sampling mask in the midpoint-offset domain.

Joint recovery model

Lowering costs while ensuring time-lapse repeatability are the main challenges in the design of seismic data monitoring systems used to optimize reservoir management and safeguard geologic carbon storage. Both challenges can be met by inverting sparsely sampled baseline and monitoring data jointly. For time-lapse acquisition with a single monitor survey, this entails inverting

$$\mathbf{b} = \mathcal{A}(\mathbf{Z}) \quad \text{with } \mathcal{A}(\cdot) = \begin{bmatrix} \mathcal{A}_1 & \mathcal{A}_1 & 0 \\ \mathcal{A}_2 & 0 & \mathcal{A}_2 \end{bmatrix}(\cdot). \tag{2}$$

In this JRM, the linear operators, $\mathcal{A}_j$, $j = 1,2$, stand for the combined action of converting monochromatic time-lapse data from the midpoint-offset domain to the source-receiver domain, followed by trace collection with the acquisition geometries defined by the binary sampling masks, $\mathbf{M}_j$, $j = 1,2$ with $j = 1$ and $j = 2$ masks for the baseline/monitor surveys. With this model, time-lapse data $\mathbf{b}$, which contain the baseline $\mathbf{b}_1$ and monitor data $\mathbf{b}_2$, are linearly related to $\mathbf{Z}$, which contains matrices for the unknown densely sampled common component $\mathbf{Z}_0$ and innovations with respect to this common component, $\mathbf{Z}_j$, $j = 1,2$. Compared to recovering the baseline/monitor surveys separately, the JRM produces repeatable results from non-replicated (Kumar et al., 2017; Oghenekohwo et al., 2017; Wason et al., 2017), noncalibrated (Oghenekohwo and Herrmann, 2017), and noisy (Tian et al., 2018) time-lapse data. These enhanced results are due to the improved recovery of the fictitious common component, and therefore, better-resolved vintages and time-lapse differences.

Time-lapse optimized mask generation

Based on the success of the JRM, we carry the argument of minimizing the SGR a step further by optimizing this quantity for the baseline/monitoring surveys. Because $\mathbf{Z}_0$ is observed by both surveys, the set of sampling points $\{\mathbf{M}_0\}$ equals the union $\{\mathbf{M}_0\} = \{\mathbf{M}_1\} \cup \{\mathbf{M}_2\}$. When surveys are replicated, $\{\mathbf{M}_0\} = \{\mathbf{M}_1\} = \{\mathbf{M}_2\}$. However, $\mathbf{M}_0$ becomes larger when the baseline and monitor surveys are not replicated, which explains why the common component is better resolved when the surveys are not replicated.

Although equation 1 leads to improved sampling masks for individual surveys, it does not exploit the fact that the common component is observed by all surveys. For this reason, we propose an optimization procedure with respect to $\mathbf{M}_1$ and $\mathbf{M}_2$ with an objective that also includes the SGR for the common component. To avoid the generation of poor sampling masks, we follow a min-max principle where the maximum — i.e., the ℓ_∞-norm — of the SGRs for the common and innovation components is minimized. To compensate for likely smaller SGRs for the common component when the surveys do not overlap ($\{\mathbf{M}_0\} > \{\mathbf{M}_1\}, \{\mathbf{M}_2\}$), we also introduce a scaling. We base this scaling on the property (see Definition 3.1 in Hoory et al., 2006; Bhojanapalli and Jain, 2014) that the second singular value of d-regular graphs — i.e., seismic data sampling masks with d nonzero entries per midpoint or offset — scales with $\sqrt{d}$. Given this scaling, we propose to minimize the following constrained optimization problem, for $j = 1,2$:

$$\begin{aligned} &\underset{\mathbf{M}_1,\mathbf{M}_2}{\text{minimize}}\ \mathcal{L}(\mathbf{M}_1,\mathbf{M}_2) \\ &\text{subject to } \{\mathbf{M}_0\} = \{\mathbf{M}_1\} \cup \{\mathbf{M}_2\}, \quad \mathbf{M}_j \in \mathcal{C}_j, \end{aligned} \tag{3}$$

with $\mathcal{L}(\mathbf{M}_1,\mathbf{M}_2) = \|[\mathcal{L}(\mathbf{M}_0), \sqrt{((\mathbf{M}_1)/(\mathbf{M}_0))}\mathcal{L}(\mathbf{M}_1), \sqrt{((\mathbf{M}_2)/(\mathbf{M}_0))}\mathcal{L}(\mathbf{M}_2)]\|_\infty$. As previously, the minimization is subject to constraints, $\mathcal{C}_j, j = 1,2$, with a slight abuse of notation, representing the cardinality, binary mask, and maximum gap constraints for the baseline and the monitor surveys, respectively.

Figure 2 shows the deployment of the proposed time-lapse acquisition design and how to recover the fully sampled time-lapse data jointly. To calculate the optimized source locations for the baseline and monitor surveys, we solve the optimization problem in equation 3. After collecting seismic data traces with the optimized (by minimizing the SGRs) acquisition, we recover fully sampled time-lapse data by inverting the system of equations included in equation 2 with structure promotion (Kumar et al., 2017). To produce time-lapse sampling masks, we use simulated annealing as proposed by Zhang et al. (2022) but with the following differences: (1) randomly perturbed masks are drawn for each survey independently, (2) the compound objectives and constraints of equation 3 are used, and (3) the sample points to be relocated are allowed to move more freely than during jitter sampling, which allows us to better explore candidate sampling masks. Figure 3 shows how the algorithm progresses in very early iterations when initialized with a replicated jittered subsampled (removing 80% of the sources) acquisition. From Figures 2 and 3a, we observe that the colocated source positions (denoted by the black dots) are gradually replaced with noncoincident source locations for the baseline (the blue dots) and monitor surveys (the red dots). Even though the objective of equation 3 decreases nonmonotonically (see Figure 3b), the reconstruction signal-to-noise ratio (S/N) increases for the baseline and monitor surveys for the selected points.

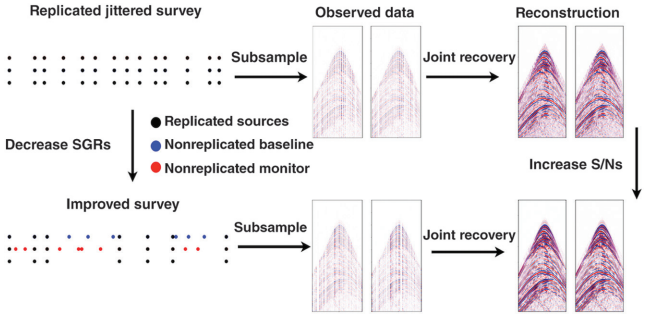

Figure 2. Illustration of the proposed optimized time-lapse acquisition design. Optimized source locations for the baseline and the monitor surveys are calculated first with equation 3, followed by collecting sparse samples in the field. Fully sampled time-lapse data are obtained by inverting the system of equations in equation 2 with structure promotion (Kumar et al., 2017). The black dots of the sampling masks plotted on the left represent the replicated source positions. The blue and red dots correspond to the nonreplicated source locations for the baseline and the monitor surveys, respectively. To better highlight the replacement of colocated with noncoincident source locations after the SGR minimization, we only display a representative subset of the actual nonoptimized and optimized source locations.

NUMERICAL VALIDATION

To confirm the benefits of the optimized acquisition, we consider time-lapse data, which differ by a complex gas cloud (Jones et al., 2012; Wason et al., 2017). Using finite differences (Louboutin et al., 2019, 2022; Witte et al., 2019; Luporini et al., 2020), fully sampled (split spread) 2D baseline and monitor surveys are simulated, each consisting of 300 sources/receivers sampled at 12.5 m. By using a single jittered subsampling mask, 80% of the sources are removed, yielding an average source sampling rate of 62.5 m with 100% overlap. After running 40,000 iterations of the simulated annealing algorithm, the SGRs of the baseline/monitor surveys decrease from

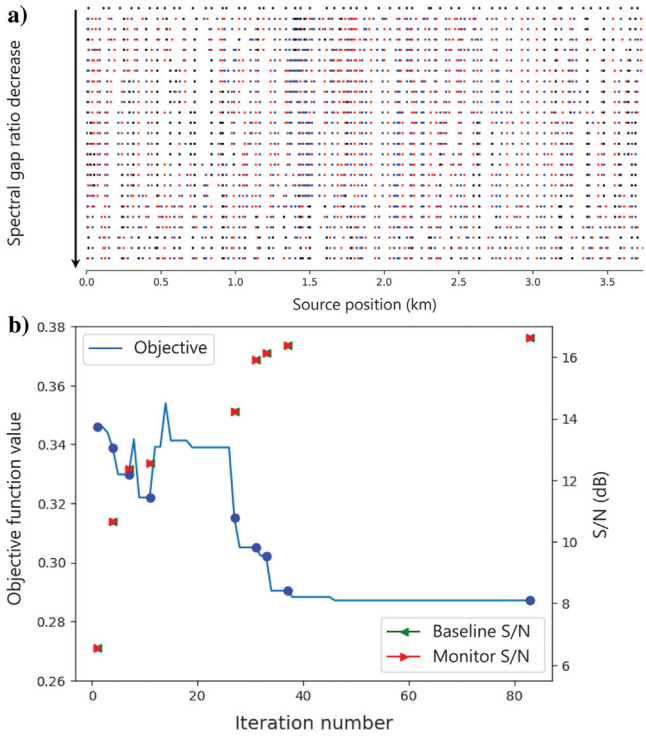

Figure 3. Automatic time-lapse sampling mask generation. (a) Starting from a jittered replicated sampling mask, the algorithm produces masks that have smaller SGRs but are no longer replicated. The overlap ratio decreases from 100% to 39%. The color scheme for markers remains consistent with Figure 2. (b) Nonmonotonically decaying objective and reconstruction S/N evaluated at points where the objective decreased by more than 0.003.

0.346 to 0.268 and 0.262, respectively. The reduction in the overlap ratio (to 22%) leads to improvement in wavefield recovery via matrix completion (Kumar et al., 2015, 2017), which results in better S/Ns for the baseline survey from 6.55 to 17.03 dB and the monitor survey from 6.67 to 16.99 dB, as shown in Figure 4. For the reasons explained by Oghenekohwo et al. (2017) and Wason et al. (2017), time-lapse difference plots are not included because the benefits of exact replication vanish when acquisition geometries undergo relatively small (1–2 m) random shifts.

Although these improvements are encouraging, the proposed optimization is approximate and the produced binary masks will be different for different starting masks. To investigate this effect, 30 overlapping jittered masks are generated by removing 75% of the sources. By reducing the overlap to $29\% \pm 8\%$, the optimized masks improve the SGRs, as can be observed from the violin plots in Figure 5a. As previously, the reductions in SGRs translate into improved S/Ns, as shown in Figure 5b. Compared with the box plots, the violin plots display the entire distribution including lines for the median (the long dashes) and the first and third quartiles (the short dashes). We can make the following observations: (1) the SGRs for the baseline/monitor surveys decrease significantly; (2) because of the larger number of sampled sources, the SGR for the common component is smaller and more narrowly distributed; (3) the distribution of the SGRs of the baseline/monitor surveys is also narrow compared with one of the initial jittered binary sampling masks; and (4) the S/Ns for the recovered baseline/monitor surveys improve significantly.

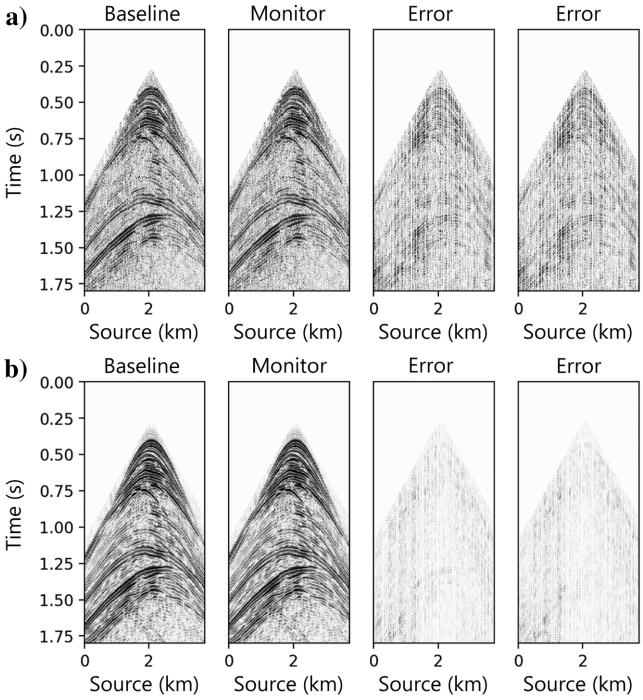

Figure 4. Time-lapse wavefield reconstruction in the time domain. (a) Wavefield reconstruction from 80% jittered subsampling for the baseline survey S/N = 6.55 dB, monitor survey S/N = 6.67 dB, and errors between the ground truth and the reconstructed wavefields. (b) The same but with optimized sampling masks, yielding improved recovery baseline/monitor surveys with S/N = 17.03 and 16.99 dB, respectively.

Even though the preceding results are encouraging and consistent with published reports that claim benefits of the JRM (Oghenekohwo et al., 2017; Wason et al., 2017; Yin et al., 2023), further scrutiny is in order. To this end, additional experiments were conducted to better understand the robustness of the proposed methodology. Aside from predictable behavior for different starting masks (Figure 5), we also found that optimized SGRs are relatively insensitive to different runs of the simulated annealing algorithm and random perturbations in the optimized masks. The first observation implies that although the simulated annealing algorithm may produce different masks, the SGRs remain very close, yielding wavefield reconstructions of near-equal quality. The second observation indicates that postplot errors by single gridpoint shifts (12.5 m) in the worst scenario offset the gains made by the optimization. However, on average, improvements are mostly preserved although with higher variability.

The observed robustness of the presented method is consistent with the reported behavior of the JRM. Even though we only consider the on-the-grid case, the argument can be made that improvements will carry over to the off-the-grid situation (López et al., 2016; Oghenekohwo and Herrmann, 2017; Wason et al., 2017). However, to turn this claim into a more solid argument, we would have to extend the presented approach to the infinite-dimensional case, which is beyond the scope of this paper.

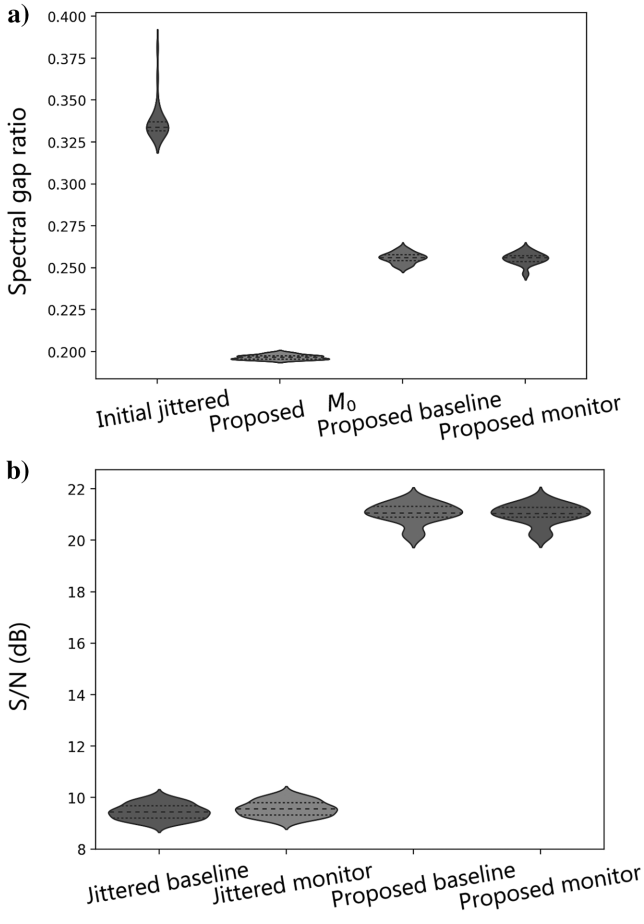

Figure 5. Violin plots for the (a) SGRs and (b) recovery S/Ns for 30 independent experiments. These experiments show systematic reductions in SGR and significantly improve reconstruction S/Ns for optimized surveys.

CONCLUSION

Acquisition costs form a major impediment to time-lapse seismic data. To reduce these costs while ensuring time-lapse repeatability, a novel acquisition optimization scheme was proposed that produces binary sampling masks that favor wavefield reconstruction with the JRM. Optimized sampling masks were generated automatically by minimizing a new objective function consisting of SGRs for the baseline/monitor surveys and the common component shared by the surveys. Aside from allowing for wave-simulation-free, and therefore computationally feasible, optimized acquisition design, the proposed method also reaffirms the suggestion that deliberate relaxation of survey replication may lead to improved quality of jointly inverted surveys. This claim is solely based on connectivity arguments for the acquisition geometries associated with the baseline/monitor surveys and the common component. Because the SGR is extremely cheap to evaluate, it lends itself very well to be extended to multiple monitoring surveys and three dimensions. As long as the time-lapse acquisition geometries are relatively well calibrated — i.e., errors between actual and assumed geometries are small — our simulation-free survey design methodology also eliminates the need for cumbersome 4D processing to a large degree. It enables low-cost surveys and uses the JRM to accurately invert for fully sampled repeatable time-lapse data without insisting on replicating the surveys in the field. The recovered data can subsequently be imaged and inverted to extract changes in the reservoir's elastic properties. The proposed method also should be capable of accommodating preexisting constraints in the field, including restricted areas where no source/receiver can be placed due to production platforms, private properties, or governmental minimum source/receiver line distance regulations. In principle, these additional constraints can be incorporated to refine the search space of the simulated annealing algorithm. Off-the-grid acquisition geometries are also conducive to being improved by SGRs, but we will leave these extensions to future work.

ACKNOWLEDGMENTS

This research was carried out with the support of the Georgia Research Alliance and partners of the ML4Seismic Center. This work was supported in part by the U.S. National Science Foundation grant OAC 2203821.

DATA AND MATERIALS AVAILABILITY

Data associated with this research are available and can be obtained by contacting the corresponding author.

REFERENCES

Bhojanapalli, S., and P. Jain, 2014, Universal matrix completion: International Conference on Machine Learning, 1881–1889.

Hennenfent, G., and F. J. Herrmann, 2008, Simply denoise: Wavefield reconstruction via jittered undersampling: Geophysics, **73**, no. 3, V19–V28, doi: 10.1190/1.2841038.

Herrmann, F. J., 2010, Randomized sampling and sparsity: Getting more information from fewer samples: Geophysics, **75**, no. 6, WB173–WB187, doi: 10.1190/1.3506147.

Herrmann, F. J., and G. Hennenfent, 2008, Non-parametric seismic data recovery with curvelet frames: Geophysical Journal International, **173**, 233–248, doi: 10.1111/j.1365-246X.2007.03698.x.

Hoory, S., N. Linial, and A. Wigderson, 2006, Expander graphs and their applications: Bulletin of the American Mathematical Society, **43**, 439–562, doi: 10.1090/S0273-0979-06-01126-8.

Jones, C. E., J. A. Edgar, J. I. Selvage, and H. Crook, 2012, Building complex synthetic models to evaluate acquisition geometries and velocity inversion technologies: 74th Annual International Conference and Exhibition, EAGE, Extended Abstracts, cp-293, doi: 10.3997/2214-4609.20148575.

Kumar, R., C. da Silva, O. Akalin, A. Y. Aravkin, H. Mansour, B. Recht, and F. J. Herrmann, 2015, Efficient matrix completion for seismic data reconstruction: Geophysics, **80**, no. 5, V97–V114, doi: 10.1190/geo2014-0369.1.

Kumar, R., H. Wason, S. Sharan, and F. J. Herrmann, 2017, Highly repeatable 3D compressive full-azimuth towed-streamer time-lapse acquisition — A numerical feasibility study at scale: The Leading Edge, **36**, 677–687, doi: 10.1190/tle36080677.1.

López, O., R. Kumar, N. Moldoveanu, and F. J. Herrmann, 2023, Spectral gap-based seismic survey design: IEEE Transactions on Geoscience and Remote Sensing, **61**, 5901809, doi: 10.1109/TGRS.2023.3237464.

López, O., R. Kumar, Ö. Yılmaz, and F. J. Herrmann, 2016, Off-the-grid low-rank matrix recovery and seismic data reconstruction: IEEE Journal of Selected Topics in Signal Processing, **10**, 658–671, doi: 10.1109/JSTSP.2016.2555482.

Louboutin, M., M. Lange, F. Luporini, N. Kukreja, P. A. Witte, F. J. Herrmann, P. Velesko, and G. J. Gorman, 2019, Devito (v3.1.0): An embedded domain-specific language for finite differences and geophysical exploration: Geoscientific Model Development, **12**, 1165–1187, doi: 10.5194/gmd-12-1165-2019.

Louboutin, M., P. Witte, Z. Yin, H. Modzelewski, and F. Herrmann, 2022, slimgroup/judi.jl: v3.2.1, doi: 10.5281/zenodo.7429592.

Luporini, F., M. Louboutin, M. Lange, N. Kukreja, P. Witte, J. Hückelheim, C. Yount, P. H. J. Kelly, F. J. Herrmann, and G. J. Gorman, 2020, Architecture and performance of Devito, a system for automated stencil computation: ACM Transactions on Mathematical Software, **46**, 1–28, doi: 10.1145/3374916.

Mosher, C., C. Li, L. Morley, Y. Ji, F. Janiszewski, R. Olson, and J. Brewer, 2014, Increasing the efficiency of seismic data acquisition via compressive sensing: The Leading Edge, **33**, 386–391, doi: 10.1190/tle33040386.1.

Obermeier, R., and J. A. Martinez-Lorenzo, 2017, Sensing matrix design via mutual coherence minimization for electromagnetic compressive imaging applications: IEEE Transactions on Computational Imaging, **3**, 217–229, doi: 10.1109/TCI.2017.2671398.

Oghenekohwo, F., and F. J. Herrmann, 2017, Highly repeatable time-lapse seismic with distributed compressive sensing — Mitigating effects of calibration errors: The Leading Edge, **36**, 688–694, doi: 10.1190/tle36080688.1.

Oghenekohwo, F., H. Wason, E. Esser, and F. J. Herrmann, 2017, Low-cost time-lapse seismic with distributed compressive sensing — Part 1: Exploiting common information among the vintages: Geophysics, **82**, no. 3, P1–P13, doi: 10.1190/geo2016-0076.1.

Tang, W., J. Ma, and F. J. Herrmann, 2008, Optimized compressed sensing for curvelet-based seismic data reconstruction: CiteSeer.

Tian, Y., L. Wei, C. Li, S. Oppert, and G. Hennenfent, 2018, Joint sparsity recovery for noise attenuation: 88th Annual International Meeting, SEG, Expanded Abstracts, 4186–4190, doi: 10.1190/segam2018-2996474.1.

Wason, H., F. Oghenekohwo, and F. J. Herrmann, 2017, Low-cost time-lapse seismic with distributed compressive sensing — Part 2: Impact on repeatability: Geophysics, **82**, no. 3, P15–P30, doi: 10.1190/geo2016-0252.1.

Wei, L., Y. Tian, C. Li, S. Oppert, and G. Hennenfent, 2018, Improve 4D seismic interpretability with joint sparsity recovery: 88th Annual International Meeting, SEG, Expanded Abstracts, 5338–5342, doi: 10.1190/segam2018-2975383.1.

Witte, P. A., M. Louboutin, N. Kukreja, F. Luporini, M. Lange, G. J. Gorman, and F. J. Herrmann, 2019, A large-scale framework for symbolic implementations of seismic inversion algorithms in Julia: Geophysics, **84**, no. 3, F57–F71, doi: 10.1190/geo2018-0174.1.

Yin, Z., H. T. Erdinc, A. P. Gahlot, M. Louboutin, and F. J. Herrmann, 2023, Derisking geologic carbon storage from high-resolution time-lapse seismic to explainable leakage detection: The Leading Edge, **42**, 69–76, doi: 10.1190/tle42010069.1.

Zhang, Y., M. Louboutin, A. Siahkoohi, Z. Yin, R. Kumar, and F. J. Herrmann, 2022, A simulation-free seismic survey design by maximizing the spectral gap: Second International Meeting for Applied Geoscience & Energy, Expanded Abstracts, 15–20, doi: 10.1190/image2022-3751690.1.

Biographies and photographs of the authors are not available.